



Resolving the mesospheric nighttime 4.3 μm emission puzzle: New model calculations improve agreement with SABER observations

Peter A. Panka^{1,2}, Alexander A. Kutepov^{2,3}, Konstantinos S. Kalogerakis⁴, Diego Janches², James M. Russell⁵, Ladislav Rezac⁶, Artem G. Feofilov⁷, Martin G. Mlynczak⁸, and Erdal Yiğit¹

¹Department of Physics and Astronomy, George Mason University, Fairfax, Virginia, USA.

²NASA Goddard Space Flight Center, Greenbelt, MD, USA.

³The Catholic University of America, Washington, DC, USA.

⁴Center for Geospace Studies, SRI International, Menlo Park, California, USA.

⁵Center for Atmospheric Sciences, Hampton University, Hampton, VA, USA.

⁶Max Planck Institute for Solar System Research, Göttingen, Germany.

⁷Laboratoire de Météorologie Dynamique/IPSL/FX-Conseil, CNRS, Ecole Polytechnique, Université Paris-Saclay, 91128 Palaiseau, France.

⁸NASA Langley Research Center, Hampton, Virginia, USA.

Correspondence to: P. A. Panka (ppanka@masonlive.gmu.edu)

Abstract. Since 2002, SABER (Sounding of the Atmosphere using Broadband Emission Radiometry)/TIMED (Thermosphere, Ionosphere, Mesosphere, Energetics and Dynamics) has been continuously measuring the day- and nighttime infrared limb radiances of the mesosphere and lower thermosphere (MLT) in ten broadband channels. Recently, the MLT daytime temperature/pressure and CO₂ densities have been obtained self-consistently from SABER 15 μm and 4.3 μm emission observations.

- 5 However, similar nighttime data remain unprocessed due to a lack of understanding of the 4.3 μm emission generating mechanisms. A previous study suggested the “direct” transfer $\text{OH}(\nu) \Rightarrow \text{N}_2(\nu) \Rightarrow \text{CO}_2(\nu_3) \Rightarrow 4.3 \mu\text{m}$ of vibrational excitation from OH(ν) to CO₂ in the nighttime mesosphere. However, accounting for this excitation mechanism alone leads to significant under-prediction (by up to 80%) of observed 4.3 μm limb radiances. Recently, theoretical and laboratory studies have suggested an additional “indirect” nighttime channel $\text{OH}(\nu) \Rightarrow \text{O}(^1\text{D}) \Rightarrow \text{N}_2(\nu) \Rightarrow \text{CO}_2(\nu_3) \Rightarrow 4.3 \mu\text{m}$ of this energy transfer.
- 10 We implemented this new channel in our non-LTE (non-Local Thermodynamic Equilibrium) model and show that, for various latitudinal and seasonal scenarios, including this additional channel brings differences between simulated and measured nighttime SABER 4.3 μm limb radiances to (-20, +30)%. These results confirm the important role of the new mechanism as a source of the nighttime 4.3 μm emission. This finding creates new opportunities for the application of CO₂ 4.3 μm observations in the study of the energetics and dynamics of the nighttime MLT.

15 1 Introduction

The SABER (Sounding of the Atmosphere using Broadband Emission Radiometry) instrument on board the NASA TIMED (Thermosphere, Ionosphere, Mesosphere, Energetics and Dynamics) satellite (Russell III et al., 1999) measures the limb radiance of the atmosphere in ten broadband infrared (IR) channels over an altitude range that spans the mesosphere and lower



thermosphere (MLT). These measurements are aimed at retrieving various MLT parameters such as kinetic temperature, pressure, and densities of O₃, H₂O, CO₂, O, and other constituents.

Recently, daytime temperature/pressure and CO₂ densities have been obtained from the SABER 15 μm and 4.3 μm emission observations (Rezac et al., 2015) using a self-consistent two-channel retrieval approach which accounts for strong coupling between both emissions. Although CO₂ is one of the key trace constituents of the MLT, whose 15 μm emission is a main steady source of cooling in this region, up to now no observations of this constituent at nighttime are available. Additionally, CO₂ has a relatively long chemical lifetime, therefore, it can act as a tracer for dynamical transport processes, such as molecular and eddy diffusion, transport by atmospheric tides and also for determining the residual mean circulation. However, little is still known about its distribution and variability, particularly about its diurnal variation and its distribution in polar night. The extensive SABER nighttime 4.3 μm radiance observations, which is supposed to fill this knowledge gap, remain, however, still unprocessed due to a lack of understanding of physical mechanisms generating this emission. As a result, nighttime temperatures are currently retrieved independently from the SABER 15 μm channel radiances using day-night mean CO₂ densities from the WACCM (Whole Atmosphere Community Climate Model) model (Garcia et al., 2007).

A detailed study of nighttime 4.3 μm emissions was conducted in the work by López-Puertas et al. (2004) aimed at determining the dominant mechanisms of exciting CO₂(ν₃), where ν₃ is the asymmetric stretch mode that emits 4.3 μm radiation. The nighttime measurements of SABER channels 7 (4.3 μm), 8 (2.0 μm), and 9 (1.6 μm) for geomagnetically quiet conditions were analyzed, where channels 8 and 9 are sensitive to the OH(ν ≤ 9) overtone radiation from levels ν = 8–9 and ν = 3–5, respectively. López-Puertas et al. (2004) showed a positive correlation between 4.3 μm and both OH channel radiances at a tangent height of 85 km. This correlation was associated with a fast and efficient transfer (Kumer et al., 1978) of energy of vibrationally excited OH(ν) produced in the chemical reaction



first to N₂(1)



and then further to CO₂(ν₃) vibrations



(hereafter "direct" mechanism). However, using laboratory rate coefficients of corresponding reactions the authors were unable to reproduce the 4.3 μm radiance observed by SABER. Although accounting for energy transfer from OH(ν) did provide a substantial enhancement to 4.3 μm emissions, a 40% difference between simulated and observed radiance remained (for the SABER scan 22, orbit 01264, 77°N, 03 Mar 2002, which was studied in detail) for altitudes above 70 km. In order to fit measurements, on average, the authors found that 2.8–3 N₂(1) molecules (instead of the accepted value of 1) are needed to be produced after each quenching of OH(ν) molecule in reaction (R2). Alternative excitation mechanisms that were theorized to enhance the 4.3 μm radiance (i.e. via O₂ and direct energy transfer from OH to CO₂) were tested but found to be insignificant.



Recently, Sharma et al. (2015) suggested a new “indirect” mechanism of the OH vibrational energy transfer to $\text{CO}_2(\nu_3)$, i.e. $\text{OH}(\nu) \Rightarrow \text{O}(^1\text{D}) \Rightarrow \text{N}_2(\nu) \Rightarrow \text{CO}_2(\nu_3) \Rightarrow 4.3 \mu\text{m}$. Accounting for this mechanism, but only considering $\text{OH}(\nu=9)$, these authors performed simple model calculations to validate its potential for enhancing mesospheric nighttime $4.3 \mu\text{m}$ emission from CO_2 . They reported a simulated radiance enhancement between 18-55% throughout the MLT, which brought it closer to observed measurements. In a latest study, Kalogerakis et al. (2016) provided a definitive laboratory confirmation for the validity of this new mechanism.

We modified our nighttime CO_2 non-LTE model, described in the work by Shved et al. (1998), to account for the “direct” mechanism of the $\text{OH}(\nu)$ energy transfer to CO_2 in a way consistent with that of (López-Puertas et al., 2004), and then added the new “indirect” mechanism proposed by Sharma et al. (2015) and Kalogerakis et al. (2016). Confining our consideration to quiet (non-auroral) nighttime conditions to avoid accounting for interactions between charged particles and molecules, whose mechanisms still remain poorly understood, we studied in detail the impact of both the “direct” mechanism alone and the combined effect of the two mechanisms on simulated nighttime SABER $4.3 \mu\text{m}$ radiances. We compared simulated radiances with the SABER measured radiances for various latitudes and seasons and present here results of this analysis.

2 Non-LTE Model Applied

A non-LTE analysis was applied to CO_2 and OH using the non-LTE ALI-ARMS (Accelerated Lambda Iterations for Atmospheric Radiation and Molecular Spectra) code package (Kutepov et al. (1998), Gusev and Kutepov (2003), Feofilov and Kutepov (2012)), which is based on the Accelerated Lambda Iteration approach (Rybicki and Hummer, 1991).

Our CO_2 non-LTE model is described in detail by Shved et al. (1998) and Feofilov and Kutepov (2012). We modified its nighttime version to account for the “direct” mechanism, reactions (R1-R3), in a way consistent with that of López-Puertas et al. (2004) and added the “indirect” mechanism of Sharma et al. (2015) and Kalogerakis et al. (2016) as described in detail below. Our OH non-LTE model resembles that of Xu et al. (2012), however, it accounts additionally for spin-orbit states $3/2$ and $1/2$ for each of 10 vibrational levels considered with corresponding weighting functions estimated using the approach discussed in Funke and López-Puertas (2000) for NO modeling.

2.1 Model Inputs

Atmospheric pressure, temperature and O density retrieved from SABER measurements (Remsberg et al. (2008), Mlynczak et al. (2013), see also <http://saber.gats-inc.com>) were used for simulating measured radiances in this study. The main atmospheric constituents (N_2 and O_2), as well as OH and CO_2 densities, were taken from the WACCM model (Garcia et al., 2007).

2.1.1 New Mechanism of $\text{CO}_2(\nu_3)$ excitation at nighttime

Sharma et al. (2015) suggested an additional mechanism that may contribute to the $\text{CO}_2(\nu_3)$ excitation at nighttime, and discussed in detail its available experimental and theoretical evidence. According to this mechanism, highly vibrationally excited $\text{OH}(\nu)$, produced by reaction (R1), rapidly loses several quanta of vibrational excitation in collisions with $\text{O}(^3\text{P})$



through a fast, spin-allowed, vibration-to-electronic energy transfer process that produces $O(^1D)$,

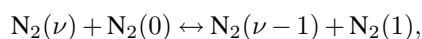


Recently, Kalogerakis et al. (2016) have presented the first laboratory demonstration of this new $OH(\nu) + O(^3P)$ relaxation pathway.

- 5 The production at nighttime of electronically excited $O(^1D)$ atoms in reaction (R4) has crucial importance. It triggers well known pumping mechanisms for daytime $4.3 \mu\text{m}$ emission (Nebel et al. (1994), Edwards et al. (1996)), where $O(^1D)$ atoms are first quenched by collisions with N_2 in a fast spin-forbidden energy transfer process



- leaving N_2 molecules with an average of 2.2 vibrational quanta, then $N_2(\nu)$ transfers its energy to ground state N_2 via a very
10 fast single quantum VV process,



which is followed by reaction (R3).

2.2 Collisional Rate Coefficients

- We use, in our CO_2 non-LTE model, the same VT and VV collisional rate coefficients for the CO_2 lower vibrational levels as
15 those of López-Puertas et al. (2004). However, a different scaling of these basic rates is applied for higher vibrational levels using the first-order perturbation theory as suggested by Shved et al. (1998).

- The reaction rate coefficients applied in this study for modeling the transfer of $OH(\nu)$ vibrational energy to the $CO_2(\nu_3)$ mode are displayed in Table 1. The total chemical production rate of $OH(\nu)$ in reaction (R1) was taken from Sander et al. (2011) and the associated branching ratios for ν were taken from Adler-Golden (1997). The rate coefficient for reaction (R2) was taken
20 from Adler-Golden (1997), measured at room temperature, and multiplied by a low temperature factor of 1.4 (Lacoursière et al., 2003) for MLT regions. Sharma et al. (2015) estimated a rate coefficient of reaction (R4) for $OH(\nu=9)$ as $(2.3 \pm 1) \times 10^{-10} \text{ cm}^3 \text{ s}^{-1}$ near 200 K for mesospheric temperatures. In this study, we applied this coefficient for each $OH(\nu \geq 5)$. Additionally, $OH(\nu < 5)$ collisions with $O(^3P)$ are considered completely inelastic and, therefore, we used for them the rate coefficient $3 \times 10^{-11} \text{ cm}^3 \text{ s}^{-1}$ from Caridade et al. (2013). The rate coefficient for the reaction $O(^1D) + N_2(0)$ (reaction (R5) in Table
25 1) was taken from Sander et al. (2011) with accounting for the fact that 33% of the electronic energy is transferred to N_2 (Slanger and Black, 1974) producing, on average, 2.2 N_2 vibrational quanta. The rate coefficient for the reaction $OH(\nu \leq 10) + O_2(0)$ (reaction (R6) in Table 1) was taken from Adler-Golden (1997) and was scaled by a factor of 1.18 to account for MLT temperatures (Lacoursière et al. (2003), Thiebaud et al. (2010)).



3 Modeling Results

3.1 Vibrational Temperatures

The non-LTE population n_ν of a molecular vibrational level ν is usually described by its vibrational temperature, T_ν . From the Boltzmann formula,

$$5 \quad \frac{n_\nu}{n_0} = \frac{g_\nu}{g_0} \exp\left[-\frac{E_\nu - E_0}{kT_\nu}\right],$$

where T_ν is defined by the degree of excitation of level ν against the ground level 0 and g_ν and E_ν are the statistical weight and the energy of level ν , respectively. If $T_\nu = T_{kin}$ then level ν is in LTE.

Figure 1 shows the vibrational temperatures of the CO₂ levels of four isotopes, giving origin to 4.3 μm bands, which dominate the SABER nighttime signal (López-Puertas et al., 2004). These results were obtained for SABER scan 22, orbit
10 01264, 77°N, 03 March 2002. The same scan was used for the detailed analysis presented in the work by López-Puertas et al. (2004). The kinetic temperature retrieved for this scan from the SABER 15 μm radiances and vibrational temperature of N₂(1) are also shown. Dashed and solid lines in Fig. 1 represent simulations with accounting for “direct” mechanism (reactions (R1-R3) alone) and with additionally implemented “indirect” mechanism (reaction (R4)), respectively.

Vibrational temperatures of CO₂ levels and N₂(1) depart from LTE around 65 km. The additional accounting for reaction
15 (R4) provides an increase of vibrational temperatures in the MLT. At 90 km, the T_ν of 626(00011) increases by 22 K, that of N₂(1) increases by 26 K, whereas the minor isotopes (636, 628, and 627) and 626(01111) show a smaller enhancement of 3-8 K. In both simulations, CO₂(00011) of main isotope 626 and N₂(1) have almost identical vibrational temperatures up to ~87 km which is caused by an efficient VV exchange reaction (R3).

3.2 Comparison of Measured and Simulated Radiances

Figure 2 displays the measured SABER channel 7 (4.3 μm) radiance (black) for the scan described in Sect. 3.1. The violet
20 curve in this figure represents the 4.3 μm simulated signal for this scan obtained by López-Puertas et al. (2004), long dash curve in Fig. 10 of this paper, with accounting for contribution in the channel 7 radiance emitted by OH($\nu \leq 10$), and applying reactions (R1-R3) only (“direct” mechanism). Our calculations for this scan with accounting for “direct” mechanism alone are given by the blue curve. They also account for OH emission contribution and use inputs identical to those of (López-Puertas
25 et al., 2004) except for OH densities. Whereas López-Puertas et al. (2004) retrieved OH densities from SABER measurements, OH for this and our calculations discussed below are taken from WACCM results (Garcia et al., 2007). Our calculations reproduce the result of (López-Puertas et al., 2004) very well between 70-95 km. There is a minor discrepancy around 87 km, where the OH peak resides, which is likely a result of OH density differences. Orange, red and green curves in Fig. 2 show
30 results of our calculations with accounting for the combined effect of both “direct”, reactions (R1-R3), and “indirect” reaction (R4) mechanisms. The three radiance profiles correspond to the range of rate coefficients reaction (R4) (see Table 1) within uncertainty limits estimated by Sharma et al. (2015). Accounting for the “indirect” mechanism “on top” of the “direct” one



produces strong enhancement of $4.3 \mu\text{m}$ radiation for all runs in which the results display agreement to within $(-23, +6.5)\%$, $(-12, +10)\%$, and $(-4, +20)\%$ of SABER measurements, for rate coefficients $1.3, 2.3,$ and $3.3 \times 10^{-10} \text{ cm}^3\text{sec}^{-1}$, respectively.

We also modeled $4.3 \mu\text{m}$ emissions for two representative nights (solar zenith angle (SZA) greater than 100°) at solstice, 15 July 2010 (311 scans), and equinox, 10 October 2008 (524 scans), which are shown in Fig. 3. The residual $4.3 \mu\text{m}$ radiance (simulated-measured)/measured is displayed with accounting for the “direct” mechanism alone (Fig. 3a and 3c) and when both “direct” and “indirect” mechanisms are included (Fig. 3b and 3d). Figures 3a and 3b display nighttime scans taken on 15 July 2010. When only the “direct” mechanism is considered (Fig. 3a), SABER measurements are reproduced to within 20% for southern latitudes and 30% for northern latitudes up to 75 km. Above 75 km, SABER measurements are shown to be gradually under-predicted from 30-80% for all latitudes, where the larger differences occur at higher altitudes. When both “direct” and “indirect” mechanisms are included (Fig. 3b), the simulated radiation is in agreement with SABER measurements to within $(-10, +20)\%$ for the majority of mid- and tropical latitudes above 90 km. Below 90 km for mid- and tropical latitudes, simulations predict SABER measurement to within $(-20, +10)\%$. The “indirect” mechanism enhances radiances from 20% at 80 km to 80% at 100 km. For higher latitudes between 60°S and 80°S , simulated emission show good agreement with measurements up to 95 km. However, above 95 km, the $4.3 \mu\text{m}$ emissions are still under-predicted between 20% and 60%. This mismatched predictions may be hardly associated with any effects related to the geomagnetic activity since the kp index (<4) and the F10.7 index (≈ 75) were low on this particular day. A more detailed investigation of this narrow altitude/latitude region is needed and will be performed in later studies.

Figures 3c and 3d display nighttime scans taken on 10 October 2008. Figure 3c shows agreement with SABER measurements to within 30% up to 75 km for all latitudes. Above 75 km, SABER measurements are shown to be gradually under-predicted from 40-70%, where percentages increase with higher altitudes. In the tropical regions, however, the disparity between simulated and SABER measurements is slightly greater at all altitudes compared to other regions. When both “direct” and “indirect” mechanisms are included (Fig. 3d), the simulated radiation is in agreement with SABER measurements to within $(-20, +10)\%$ for southern latitudes and $(-10, +40)\%$ for northern latitudes from 65-110 km. In both regions, radiance enhancements range from 20-30% below 80 km to up to 80-100% above 100 km. High atomic oxygen densities in some regions could be a result of the over-predictions for $4.3 \mu\text{m}$ emission modeling. In addition, unlike the solstice scans modeled in Fig. 3a and 3b, high latitude regions do not show any large under-predictions for equinox scenarios. Modeling emissions for alternative solstice and equinox nights, i.e. January and April, showed similar results as the nights modeled in Fig. 3.

Additionally, atomic oxygen densities retrieved by SABER have been reported to be at least 30% larger than other observations (Kaufmann et al., 2014). We found that lowering the atomic oxygen density by 50% reduces the $4.3 \mu\text{m}$ emission enhancement for all atmospheric scenarios, on average, by 5-20%, where the larger percentage differences occur at higher altitudes.



4 Conclusions

Kumer et al. (1978) pointed out a fast and efficient transfer $\text{OH}(\nu) \Rightarrow \text{N}_2(\nu) \Rightarrow \text{CO}_2(\nu_3)$ of vibrational energy of chemically produced $\text{OH}(\nu)$ to the $\text{CO}_2(\nu_3)$ vibrations in the nighttime mesosphere. The effect of this mechanism on the SABER nighttime 4.3 μm emissions was studied in detail by López-Puertas et al. (2004), who showed that in order to match observations, an additional enhancement is needed that would be equivalent to the production of 2.8-3 $\text{N}_2(1)$ molecules for each quenching reaction $\text{OH}(\nu)+\text{N}_2(0)$. This finding was a clear indication that the elusive pumping mechanisms of the $\text{CO}_2(\nu_3)$ vibrations needed to be identified and accounted for. Recently, Sharma et al. (2015) suggested a new alternative “indirect” channel of the $\text{OH}(\nu)$ energy transfer to the $\text{CO}_2(\nu_3)$ vibrations $\text{OH}(\nu) \Rightarrow \text{O}(^1\text{D}) \Rightarrow \text{N}_2(\nu) \Rightarrow \text{CO}_2(\nu_3)$ and showed that it may provide an additional enhancement of the MLT nighttime 4.3 μm emission. Kalogerakis et al. (2016) provided a definitive laboratory confirmation for the validity of this new mechanism for $\text{OH}(\nu=9)+\text{O}$. We added this new “indirect” $\text{OH}(\nu)$ energy transfer channel to the “direct” mechanism in our non-LTE model of the nighttime CO_2 emissions assuming that the “indirect” rate coefficient is independent of the OH vibrational level. We studied in detail the impact of these mechanisms on simulated SABER/TIMED nighttime 4.3 μm limb radiances and found that, while accounting for the “direct” mechanism alone leads to under-predicting the SABER measured radiances by up to 80%, the addition of the new “indirect” channel results in a significant reduction of these differences bringing them to (-20, +30)% for the majority of latitudes during equinox and solstice nights. This significant improvement suggests that the missing nighttime mechanism of $\text{CO}_2(\nu_3)$ pumping has finally been identified. Further improvements will require optimizing the set of rate coefficients used for $\text{OH}(\nu)$ relaxation by $\text{O}(^3\text{P})$ and O_2 at mesospheric temperatures and, in particular, understanding the dependence of the indirect mechanism on the OH vibrational level. Relevant laboratory measurements and theoretical calculations are sorely needed to understand these relaxation rates and the quantitative details of the applicable mechanistic pathways. Nevertheless, results presented here clearly demonstrate significant progress in understanding the generation mechanisms of the nighttime CO_2 4.3 μm emission and represent an important step towards developing the algorithm(s) suitable for retrieving CO_2 densities in the MLT from the SABER nighttime limb radiances.

Acknowledgements. We would like to thank Ramesh Sharma for his helpful comments and productive collaboration with the new nighttime mechanism implementation. The work by P.A.P was supported by the NASA grant NNX14AN71G. The work by A.A.K. was supported by the NSF grant 1301762 and the NASA grant NNX15AN08G. The contributions of K.S.K were supported by NSF Grant 1441896.



References

- Adler-Golden, S.: Kinetic parameters for OH nightglow modeling consistent with recent laboratory measurements, *Journal of Geophysical Research*, 102, 19 969–19 976, doi:10.1029/97JA01622, 1997.
- Caridade, P. J. S. B., Horta, J.-Z. J., and Varandas, A. J. C.: Implications of the O+OH reaction in hydroxyl nightglow modeling, *Atmospheric Chemistry and Physics*, 13, 1–13, 2013.
- Edwards, D. P., Kumer, J. B., López-Puertas, M., Mlynczak, M. G., Gopalan, A., Gille, J. C., and Roche, A.: Non-local thermodynamic equilibrium limb radiance near 10 μm as measured by UARS CLAES, *Journal of Geophysical Research: Atmospheres*, 101, 26 577–26 588, doi:10.1029/96JD02133, <http://dx.doi.org/10.1029/96JD02133>, 1996.
- Feofilov, A. G. and Kutepov, A. A.: Infrared Radiation in the Mesosphere and Lower Thermosphere: Energetic Effects and Remote Sensing, *Surveys in Geophysics*, 33, 1231–1280, doi:10.1007/s10712-012-9204-0, <http://link.springer.com/10.1007/s10712-012-9204-0>, 2012.
- Funke, B. and López-Puertas, M.: Nonlocal thermodynamic equilibrium vibrational, rotational, and spin state distribution of NO($\nu=0, 1, 2$) under quiescent atmospheric conditions, *Journal of Geophysical Research: Atmospheres*, 105, 4409–4426, 2000.
- Garcia, R. R., Marsh, D. R., Kinnison, D. E., Boville, B. A., and Sassi, F.: Simulation of secular trends in the middle atmosphere, 1950–2003, *Journal of Geophysical Research Atmospheres*, 112, 1–23, doi:10.1029/2006JD007485, 2007.
- Gusev, O. A. and Kutepov, A. A.: Non-LTE Gas in Planetary Atmospheres, in: *Stellar Atmosphere Modeling*, edited by Hubeny, I., Mihalas, D., and Werner, K., vol. 288 of *Astronomical Society of the Pacific Conference Series*, pp. 318–330, 2003.
- Kalogerakis, K. S., Smith, G. P., and Copeland, R. A.: Collisional removal of OH($X^2\Pi$, $v=9$) by O, O₂, O₃, N₂, and CO₂, *Journal of Geophysical Research*, 116, doi:10.1029/2011JD015734, <http://doi.wiley.com/10.1029/2011JD015734>, 2011.
- Kalogerakis, K. S., Matsiev, D., Sharma, R. D., and Wintersteiner, P. P.: Resolving the mesospheric nighttime 4.3 μm emission puzzle: Laboratory demonstration of new mechanism for OH(ν) relaxation, *Geophysical Research Letters*, doi:10.1002/2016GL069645, <http://doi.wiley.com/10.1002/2016GL069645>, 2016.
- Kaufmann, M., Zhu, Y., Ern, M., and Riese, M.: Global distribution of atomic oxygen in the mesopause region as derived from SCIAMACHY O(¹S) green line measurements, *Geophysical Research Letters*, 41, 6274–6280, doi:10.1002/2014GL060574, <http://dx.doi.org/10.1002/2014GL060574>, 2014.
- Kumer, J. B., Stair, Jr., A. T., Wheeler, N., Baker, K. D., and Baker, D. J.: Evidence for an OH ^{ν} \rightarrow N₂ ^{ν} \rightarrow CO₂(ν_3) \rightarrow CO₂ + h ν (4.3 μm) Mechanism for 4.3- μm Airglow, *Journal of Chemical Physics*, 83, 4743–4747, 1978.
- Kutepov, A. A., Gusev, O. A., and Ogibalov, V. P.: Solution of the Non-LTE Problem for Molecular Gas in Planetary Atmospheres: Superiority of Accelerated Lambda Iteration, *Journal of Quantitative Spectroscopy and Radiative Transfer*, 60, 199–220, 1998.
- Lacoursière, J., Dyer, M. J., and Copeland, R. A.: Temperature dependence of the collisional energy transfer of OH($v=10$) between 220 and 310 K, *Journal of Chemical Physics*, 118, 1661–1666, doi:10.1063/1.1530581, 2003.
- López-Puertas, M., Garcia-Comas, M., Funke, B., Picard, R. H., Winick, J. R., Wintersteiner, P. P., Mlynczak, M. G., Mertens, C. J., Russell III, J. M., and Gordley, L. L.: Evidence for an OH(ν) excitation mechanism of CO₂ 4.3 μm nighttime emission from SABER/TIMED measurements, *Journal of Geophysical Research*, 109, 2–15, doi:10.1029/2003JD004383, 2004.
- Mlynczak, M. G., Hunt, L. A., Mast, J. C., Thomas Marshall, B., Russell, J. M., Smith, A. K., Siskind, D. E., Yee, J.-H., Mertens, C. J., Javier Martin-Torres, F., Earl Thompson, R., Drob, D. P., and Gordley, L. L.: Atomic oxygen in the mesosphere and lower thermosphere derived from SABER: Algorithm theoretical basis and measurement uncertainty, *Journal of Geophysical Research: Atmospheres*, 118, 5724–5735, doi:10.1002/jgrd.50401, <http://doi.wiley.com/10.1002/jgrd.50401>, 2013.



- Nebel, H., Wintersteiner, P. P., Picard, R. H., Winick, J. R., and Sharma, R. D.: CO₂ non-local thermodynamic equilibrium radiative excitation and infrared dayglow at 4.3 μm: Application to Spectral Infrared Rocket Experiment data, *Journal of Geophysical Research: Atmospheres*, 99, 10 409–10 419, doi:10.1029/94JD00315, <http://dx.doi.org/10.1029/94JD00315>, 1994.
- 5 Remsburg, E. E., Marshall, B. T., Garcia-Comas, M., Krueger, D., Lingenfelter, G. S., Martin-Torres, J., Mlynczak, M. G., Russell, J. M., Smith, A. K., Zhao, Y., Brown, C., Gordley, L. L., Lopez-Gonzalez, M. J., Lopez-Puertas, M., She, C. Y., Taylor, M. J., and Thompson, R. E.: Assessment of the quality of the version 1.07 temperature-versus-pressure profiles of the middle atmosphere from TIMED/SABER, *Journal of Geophysical Research Atmospheres*, 113, 1–27, doi:10.1029/2008JD010013, 2008.
- 10 Rezac, L., Kutepov, A., Russell III, J. M., Feofilov, A. G., Yue, J., and Goldberg, R. A.: Simultaneous retrieval of T(p) and CO₂ VMR from two-channel non-LTE limb radiances and application to daytime SABER/TIMED measurements, *Journal of Atmospheric and Solar-Terrestrial Physics*, 130-131, 23–42, doi:10.1016/j.jastp.2015.05.004, <http://linkinghub.elsevier.com/retrieve/pii/S1364682615000954>, 2015.
- Russell III, J. M., Mlynczak, M. G., Gordley, L. L., Tansock, Jr., J. J., and Esplin, R. W.: Overview of the SABER experiment and preliminary calibration results, *Proc. SPIE*, 3756, 277–288, doi:10.1117/12.366382, <http://dx.doi.org/10.1117/12.366382>, 1999.
- 15 Rybicki, G. B. and Hummer, D. G.: An accelerated lambda iteration method for multilevel radiative transfer. I - Non-overlapping lines with background continuum, *Astronomy and Astrophysics*, 245, 171–181, 1991.
- Sander, S. P., Abbatt, J., Barker, J. R., Burkholder, J. B., Friedl, R. R., Golden, D. M., Huie, R. E., Kolb, C. E., Kurylo, M. J., Moortgat, G. K., Orkin, V. L., and Wine, P. H.: Chemical Kinetics and Photochemical Data for Use in Atmospheric Studies, Evaluation Number 17, JPL Publication 10-6, pp. 1–684, <http://jpldataeval.jpl.nasa.gov/>, 2011.
- 20 Sharma, R. D., Wintersteiner, P. P., and Kalogerakis, K. S.: A new mechanism for OH vibrational relaxation leading to enhanced CO₂ emissions in the nocturnal mesosphere, *Geophysical Research Letters*, 42, 4639–4647, doi:10.1002/2015GL063724, 2015.
- Shved, G. M., Kutepov, A. A., and Ogibalov, V. P.: Non-local thermodynamic equilibrium in CO₂ in the middle atmosphere. I. Input data and populations of the ν₃ mode manifold states, *Journal of Atmospheric and Solar-Terrestrial Physics*, 60, 289–314, doi:10.1016/S1364-6826(97)00076-X, 1998.
- 25 Slanger, T. G. and Black, G.: Electronic-to-vibrational energy transfer efficiency in the O(¹D)-N₂ and singlet O(¹D)-CO systems, *J. Chem. Phys.*, 60, 468–477, doi:10.1063/1.1681064, 1974.
- Thiebaud, J. E., Copeland, R. A., and Kalogerakis, K. S.: Vibrational Relaxation of OH(ν = 7) with O, O₂, and H, Abstract #SA43A-1752, American Geophysical Union Fall Meeting, San Francisco, CA, 2010.
- Xu, J., Gao, H., Smith, A. K., and Zhu, Y.: Using TIMED/SABER nightglow observations to investigate hydroxyl emission mechanisms in the mesopause region, *Journal of Geophysical Research: Atmospheres*, 117, 1–22, doi:10.1029/2011JD016342, 2012.

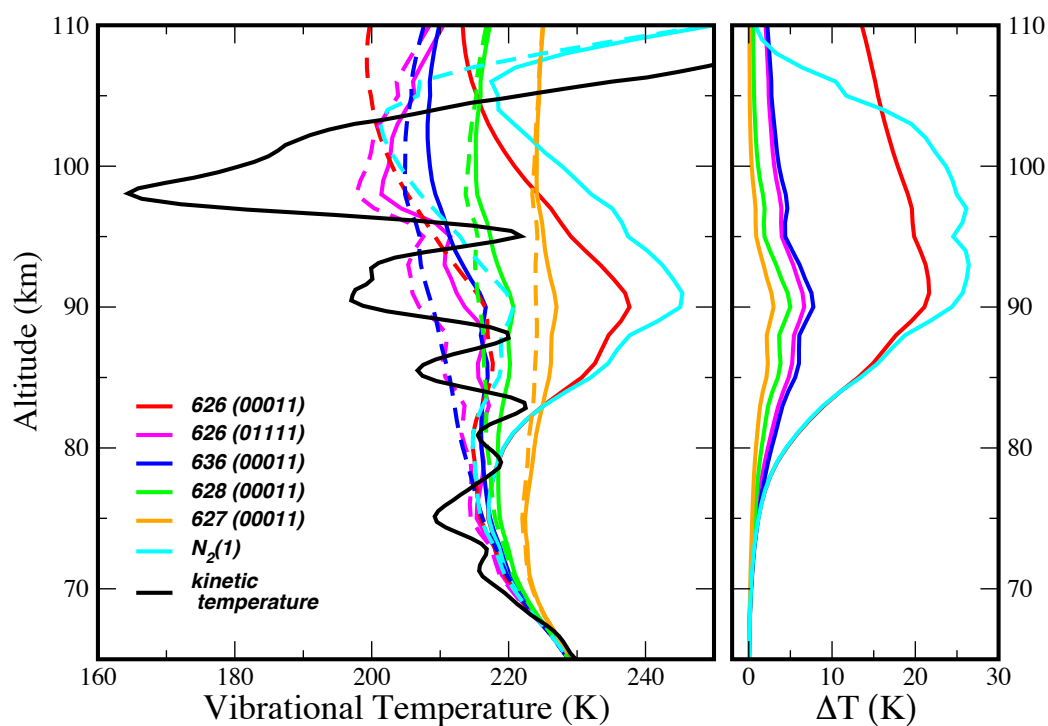


Figure 1. Nighttime vibrational temperatures of $\text{CO}_2(00011)$ of four CO_2 isotopes, $\text{CO}_2(01111)$ of main CO_2 isotope, and of $\text{N}_2(1)$ for SABER scan 22, orbit 01264, 77°N , 03 March 2002. Left: dashed lines - no reaction (R4); solid lines - with reaction (R4) included, $k_4=2.3 \times 10^{-10} \text{ cm}^3\text{s}^{-1}$. Right: vibrational temperature differences.

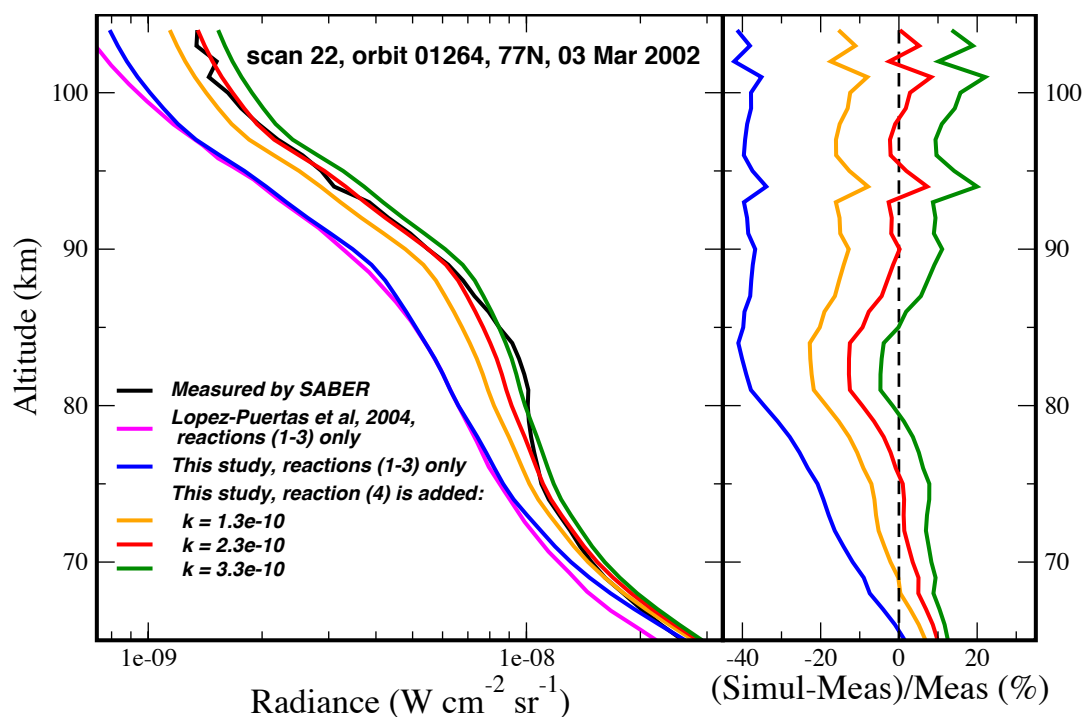


Figure 2. Left: measured and simulated SABER nighttime radiances in channel 7 (4.3 μm) for SABER scan 22, orbit 01264, 77°N, 03 March 2002. SABER measured (black); from López-Puertas et al. (2004), only reactions (R1-R3) included (violet); this study, only reactions (R1-R3) included (blue); this study, reaction (R4) added with $k_4=1.3 \times 10^{-10} \text{ cm}^3 \text{ s}^{-1}$ (orange), $k_4=2.3 \times 10^{-10} \text{ cm}^3 \text{ s}^{-1}$ (red), $k_4=3.3 \times 10^{-10} \text{ cm}^3 \text{ s}^{-1}$ (green). Right: radiance relative difference (simulated-measured)/measured in percent.

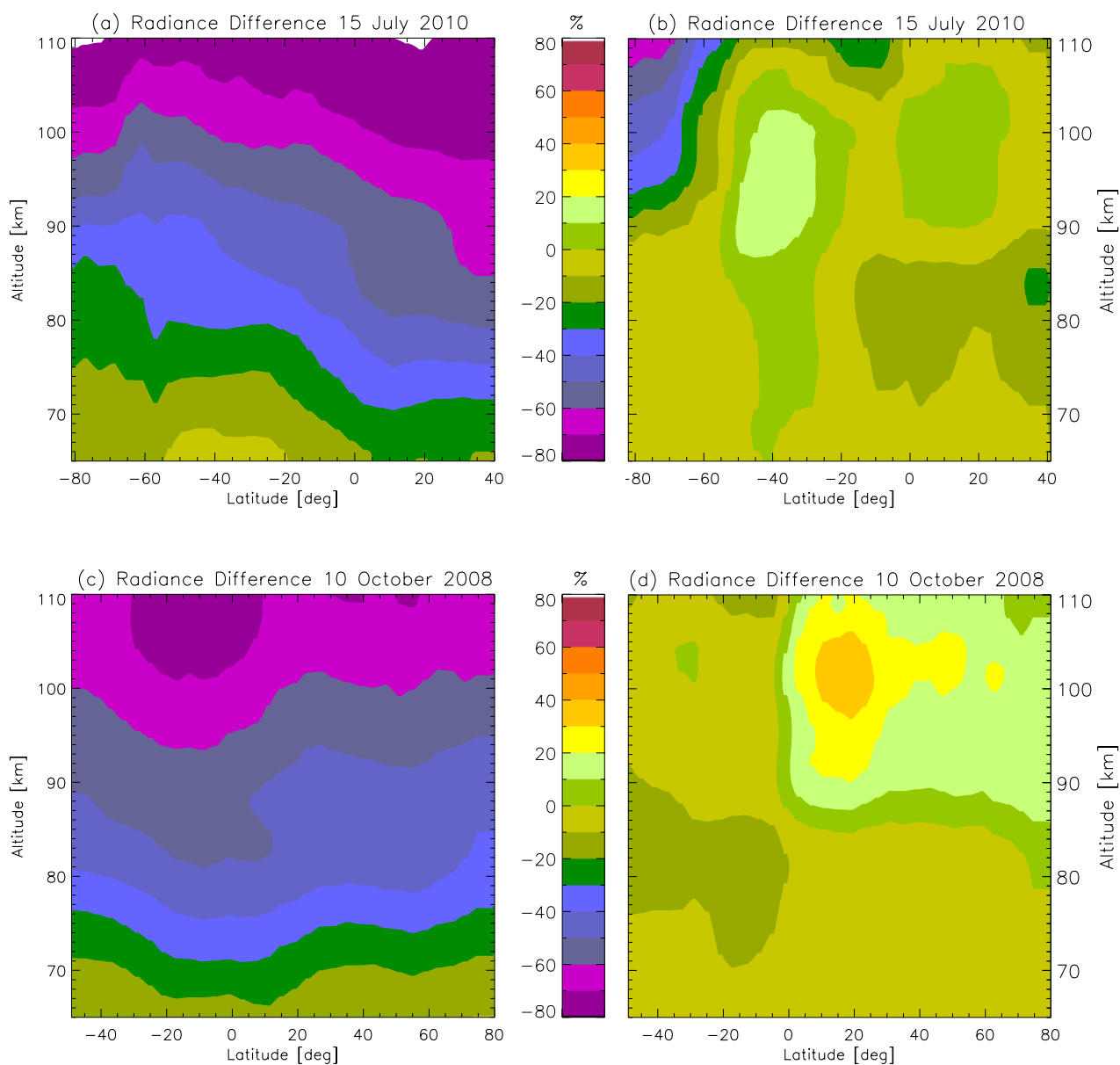


Figure 3. Residual CO₂ 4.3 μm radiance (simulated-measured)/measured. (a): without and (b): with new “indirect” mechanism (using $k_4=2.3\times 10^{-10}$ cm³s⁻¹ for reaction (R4)) suggested by Sharma et al. (2015) for all nighttime scans on 15 July 2010; (c and d): same for all nighttime scans on 10 October 2008.



Table 1. Significant collisional processes used in model

Reaction	Reaction Rate ($\text{cm}^3\text{sec}^{-1}$)	Reference
(R1) $\text{H} + \text{O}_3 \leftrightarrow \text{OH}(\nu \leq 10) + \text{O}_2$	$k_1 = f_\nu^a \times 1.4 \times 10^{-10} \exp(-470/T)$	Sander et al. (2011) & Adler-Golden (1997)
(R2) $\text{OH}(\nu \leq 10) + \text{N}_2(0) \leftrightarrow \text{OH}(\nu-1) + \text{N}_2(1)$	$k_2 = f_\nu^b \times 1.4 \times 10^{-13}$	Adler-Golden (1997) & Lacoursière et al. (2003)
(R3) $\text{N}_2(1) + \text{CO}_2(0) \leftrightarrow \text{N}_2(0) + \text{CO}_2(\nu_3)$	$k_3 = 8.91 \times 10^{-12} \times T^{-1}$	Shved et al. (1998)
(R4) $\text{OH}(\nu \geq 5) + \text{O}({}^3\text{P}) \leftrightarrow \text{OH}(0 \leq \nu' \leq \nu-5) + \text{O}({}^1\text{D})$	$k_4 = (2.3 \pm 1) \times 10^{-10}$	Kalogerakis et al. (2011) & Sharma et al. (2015)
$\text{OH}(\nu < 5) + \text{O}({}^3\text{P}) \leftrightarrow \text{OH}(0) + \text{O}({}^3\text{P})$	$k_4 = 3 \times 10^{-11}$	Caridade et al. (2013)
(R5) $\text{O}({}^1\text{D}) + \text{N}_2(0) \leftrightarrow \text{O}({}^3\text{P}) + \text{N}_2(\nu)$	$k_5 = 2.15 \times 10^{-11} \exp(110/T)$	Sander et al. (2011)
(R6) $\text{OH}(\nu \leq 10) + \text{O}_2(0) \leftrightarrow \text{OH}(\nu) + \text{O}_2(1)$	$k_6 = f_\nu^c \times 1.18 \times 10^{-13}$	Adler-Golden (1997)

^a $f_\nu(\nu=5-9) = (0.01, 0.03, 0.15, 0.34, 0.47)$

^b $f_\nu(\nu=1-10) = (0.06, 0.10, 0.17, 0.30, 0.52, 0.91, 1.6, 7, 4.8, 6)$

^c $f_\nu(\nu=1-10) = (1.9, 4, 7.7, 13, 25, 43, 102, 119, 309, 207)$